Materials Today Bio 27 (2024) 101146

Contents lists available at ScienceDirect

Materials Today Bio

journal homepage: www.journals.elsevier.com/materials-today-bio

Synergistic potential of gellan gum methacrylate and keratin hydrogel for visceral hemostasis and skin tissue regeneration

Che-Wei Lin [a,b,1], Tai-Hung Liu [b,1], Vincent Chen [b], Er-Yuan Chuang [a,**], Yu-Jui Fan [a,***], Jiashing Yu [b,*]

[a] School of Biomedical Engineering, Taipei Medical University, Taipei, 10675, Taiwan
[b] Department of Chemical Engineering, National Taiwan University, Taipei, 10617, Taiwan

ARTICLE INFO

Keywords:
Keratin
Gellan gum
Hydrogel
Wound healing
Tissue adhesive
Hemostasis

ABSTRACT

In recent years, the development of biodegradable hydrogels as an alternative over the traditional wound dressing has become increasingly significant. These specific hydrogels are able to offer suitable microenvironments to further aid the process of tissue or organ regeneration. However, application of biodegradable hydrogels in clinical medicine remains uncommon due to most biodegradable hydrogels struggle with achieving satisfactory adhesiveness property, high mechanical support and cell compatibility simultaneously. In order to overcome these constraints and enhance the applicability of biodegradable hydrogels, methods have been employed in this study.

By reacting gellan gum with methacrylic anhydride and incorporating a biodegradable protein, keratin, we endowed the hydrogels with high pliability via photo-polymerization chain extension, thereby obtaining a biodegradable hydrogel with exceptional properties. Through a series of *in vitro* tests, GGMA/keratin hydrogels exhibited great cell compatibility via providing an appropriate environment for cell proliferation. Furthermore, this hydrogel not only exhibits extraordinary adhesive ability on visceral tissues but also extends to scenarios involving skin or organ damage, offering valuable assistance in wound healing. Our design provides a suitable platform for cell proliferation and tissue regeneration, which shows prospects for future medical research and clinical applications.

1. Introduction

In clinical medicine, wound-induced bleeding and severe organ hemorrhage are often regarded as recurrent obstacles. When acute trauma results in severe blood loss, it can lead to irreversible damage and even life-threatening situations [1]. For patients with chronic diseases, the presence of wounds also poses a severe threat accompanied by delayed wound healing, continuous bleeding, and even fatal consequences due to insufficient adhesion of present dressings to tissue surfaces or merely serving as a barrier to the external environment but lacking mechanical support [2–6]. Consequently, there is a significant need to design dressings that can effectively adhere to the affected area, quickly stop bleeding, and concurrently facilitate the wound healing process. Innovative strategies aim to meet the comprehensive requirements of wound management and provide enhanced, holistic support for patient recovery [7,8]. Exploring alternative designs could lead to the development of a dressing that both rapidly achieves hemostasis and accelerates the wound healing process.

Natural biological dressings, derived from sources like collagen, gelatin, keratin, chitosan, fucoidan, sodium alginate, and collagen peptides, are extensively used to promote wound healing, aid skin repair, and stimulate tissue regeneration, offering a wide range of benefits and unique properties [9–15]. In addition, these dressings possess bioactive properties, such as antimicrobial, anti-inflammatory, and cell growth promotion, which help prevent wound expansion and support tissue regeneration [16]. Due to their natural origins, these dressings are more readily accepted by human tissues and are thus employed under various conditions for different treatments [17,18]. Despite these

* Corresponding author.
** Corresponding author.
*** Corresponding author.
E-mail addresses: eychuang@tmu.edu.tw (E.-Y. Chuang), Ray.yj.fan@tmu.edu.tw (Y.-J. Fan), jiayu@ntu.edu.tw (J. Yu).
[1] Che-Wei Lin and Tai-Hung Liu had equal contribution to this study.

https://doi.org/10.1016/j.mtbio.2024.101146
Received 5 March 2024; Received in revised form 14 June 2024; Accepted 1 July 2024
Available online 4 July 2024

benefits, traditional degradable hydrogel-based dressings made from a single material, while somewhat elastic, still face challenges due to their low mechanical strength [19–21]. Therefore, this study aims to address these limitations and enhance the mechanical strength and malleability of biodegradable hydrogels by utilizing highly-modifiable material, gellan gum, incorporating with bioactive molecule, keratin, to enhance the performance of hydrogel in medical applications.

Gellan gum (GG) is a linear polysaccharide derived from a bacterium, Sphingomonas elodea. The overall structure of gellan gum is composed of four units: 1,3-β-D-glucose, 1,4-β-D-glucuronic acid, 1,4-β-D-glucose, and 1,4-α-L-rhamnose. Additionally, it contains a carboxyl group side chain [22]. In tissue engineering and biomaterial applications, gellan gum displays versatile characteristics including acid and heat stability, adjustable mechanical strength, thermo-responsiveness, excellent biocompatibility, biodegradability, and easy functionalization [23–30]. Its broad versatility and exceptional properties, combined with its ability to synergize with other materials like agar, keratin, gelatin, and starch, present promising opportunities for innovative research in tissue engineering and biomedicine [31–35].

Keratin is an insoluble protein found in epithelial tissues, part of the fibrous structural proteins family, and prevalent in hair, feathers, claws, hooves, and the outer layer of human skin. Research shows that keratins, which vary by source, primarily have α-helical and β-folded sheet structures, with high cysteine content that enhances stability and mechanical strength through disulfide bond formation [36,37]. Their capacity for self-assembly and cross-linking makes them highly applicable in tissue engineering and biomedical fields, and their molecular structure includes crucial cell-adhesion motifs like leucine-aspartic acid-valine (LDV) and glutamic acid-aspartic acid-serine (EDS), which facilitate cell matrix binding [38–40]. Studies confirm keratin's role in promoting the adhesion of various cell types crucial for tissue repair and regeneration [13,41–45]. Furthermore, keratin-based biomaterials are beneficial in wound treatment, serving as versatile carriers that effectively deliver cells or small molecules to expedite healing [44,46–48]. Despite extensive research into keratin characteristics (such as structures and amino acid compositions), comparative studies on keratins from different sources in identical medical applications are still lacking even though keratin of different origins contain distinct variations (e.g. Hair keratin contain more α-helical structures while feather keratin contain more β-folded sheet) [36,37]. This research aims to explore the effects of keratins derived from hair and feathers *in vivo*.

In this study, we initiated a reaction between commonly-used polymer, gellan gum, and methacrylates reagent, followed by the incorporation of biodegradable keratin extracted from hair and feathers. We successfully achieved a high level of flexibility in the hydrogel via photopolymerization chain extension, leading to the preparation of biodegradable hydrogels. Through extensive mechanical and *in vitro* analysis, this type of biodegradable hydrogel shows potential in the field of wound care applications, providing a platform that faithfully replicates a realistic tissue microenvironment. Moreover, after *in vivo* evaluations on mouse skin and liver injury models, this biodegradable hydrogel not only demonstrates protective potential in skin wound healing but also extends its utility to situations involving organ damage, thus providing assistance in wound healing and regeneration.

2. Experimental section

2.1. Gellan gum methacrylate (GGMA) fabrication

Gellan gum methacrylate (GGMA) synthesis was modified from a method described in literature [49,50]. Gellan gum methacrylate (GGMA) was synthesized by the substitution reaction of gellan gum (GG) with methacrylic anhydride (MAA). 1 g of gellan gum was dissolved in 100 mL deionized water at 90 ° C for 20–30 min under constant-stirring. After fully dissolving gellan gum, the solution is slowly cooled to 50 ° C and 6 mL of MAA was then added into the solution for reaction. The pH value of solution is adjusted to maintain within the range of 8.0–9.0. After 4 h, the product solution was dialyzed using a dialysis membrane with a molecular weight cutoff of 12000–14000 Da (Thermo, USA) against deionized water for at least three days. The final product was obtained by lyophilization.

2.2. Keratin extraction

Keratin was obtained from human hair using a method previously described in literature [44]. Initially, human hair was thoroughly washed with distilled water and then immersed in a mixture of methanol and chloroform (2:1, v/v; ECHO Chemical Co., Taiwan) for 18–24 h to remove any lipid coating on the hair's surface. Subsequently, the hair was air-dried for 3 h and then soaked in an extraction solution containing 5 M urea, 25 mM Tris-HCl, 5 % 2-mercaptoethanol (β-ME), and 2.6 M thiourea at 50 °C for 72 h. The keratin solution obtained from the extraction was filtered through a 0.22 μm filter (Thermo, USA) and then centrifuged at 5000 g for 5 min at 4 °C. Finally, the supernatant was extensively dialyzed using a dialysis membrane with a molecular weight cutoff of 6000–8000 Da (Thermo, USA) for 24 h at 4 °C. The protein concentration of the extracted keratin was determined using the Protein Assay Dye Reagent (Bio-Rad, USA). The molecular weight of the keratin was confirmed through sodium dodecyl sulfate-polyacrylamide gel electrophoresis (SDS-PAGE) analysis (Fig. S1).

Feather keratin was extracted from the feather of duck (*Anas platyrhynchos* domesticus) with the reduction method (Shindai method) which is mentioned in *previously reported study* [51]. First, feathers were washed by 0.5 % (w/v) sodium dodecyl sulfate$_{(aq)}$ to remove dust. Then, the feathers were dried and cut into small filaments the size of 1–2 mm. After drying, the feather filaments were soaked in 95 % (v/v) ethanol solution for 2 h to remove the remaining lipid coating. The ethanol-immersed feather filaments were further treated with 5 % (v/v) hydrogen chloride$_{(aq)}$ (HCl) in order to break hydrogen bonding. Next, the pretreated feather filaments were immersed in an extraction solution containing 8 M urea, 0.2 M Tris-HCl, 1.66 M β-ME and 0.26 M SDS at 50 ° C, pH 9.0 for 72 h. After reaction, the solution was filtered and dialyzed using a dialysis membrane with a molecular weight cutoff of 3500 Da (Thermo, USA) for 72 h. The protein concentration of the extracted keratin was determined using the Protein Assay Dye Reagent (Bio-Rad, USA). The molecular weight of the keratin was also confirmed through SDS-PAGE analysis (Fig. S1).

2.3. GGMA-based hydrogels fabrication

For preparation of GGMA hydrogel, the lyophilized GGMA product was dissolved in deionized water to total concentration of 2 % (w/v) at 40 ° C for 1 h. The photoinitiator lithium phenyl (2,4,6-trimethylbenzoyl) phosphinate (LAP) was also added to assist the cross-linking process of hydrogel. For GGMA/HK and GGMA/FK hydrogel, the deionized water in previous procedures were substituted for respective extracted keratin solutions. And the concentration of both types of keratin were adjusted to 2 % (w/v). All of the hydrogel samples were exposed to 365 nm, 1 W ultra-violet light source for 1 min to form the hydrogels.

2.4. Circular dichroism (CD) spectroscopy & amino acid analysis

CD spectroscopy was utilized to analyze the secondary protein structure of hair and feather keratins. The diluted protein solutions (with final concentration of 0.01 mg/mL) were placed in 1.0 cm path length quartz cuvette and measured via J-810 CD spectropolarimeter (Jasco, Japan) with the range from 190 to 250 nm.

The amino acid compositions of hair and feather keratins were acquired by amino acid analysis. The samples were hydrolyzed in 6 N HCl solution at 110 °C for 24 h, and the treated samples were then analyzed via Hitachi L8900 Amino Acid Analyzer (Hitachi, Japan).

2.5. FT-IR & NMR

In order to precisely investigate the chemical composition ratio of hydrogels, Fourier transform infrared (FT-IR) spectroscopy and ^{13}C solid-state nuclear magnetic resonance (NMR) spectroscopy were employed. All sample groups were lyophilized before the aforementioned analysis. For the FT-IR spectrum, samples for analysis were prepared with potassium bromide (KBr) pellet method. Nicolet NEXUS 470 FT-IR spectrometer (Thermo/Nicolet Nexus, USA) was utilized. Spectral data were meticulously collected within the wavenumber range of 450 cm^{-1} to 4000 cm^{-1}, facilitating a comprehensive and in-depth analysis of the composition. For ^{13}C solid–state NMR, the data were obtained by Bruker AVIII 600 WB SSNMR (Bruker, Rheinstetten, Germany).

2.6. Scanning electron microscope (SEM)

To investigate the microstructure and pore characteristics of hydrogels with various mixing ratios, a comprehensive analysis was conducted using a FEI NOVA NANOSEM 230 scanning electron microscope (SEM) (NovaTM, USA) operating at an acceleration voltage of 10 kV. Before SEM imaging, the hydrogels underwent preparation, including lyophilization for 18–24 h and sputter deposition of a gold coating. SEM observations were performed at a magnification of 5000× to capture high-resolution details. Subsequently, the acquired SEM images and pore size observations were rigorously processed and analyzed using Image-J software. (Image-J 1.47, ImageJ, USA).

2.7. Characterization of pore size, pore distribution, and porosity in GGMA-based hydrogels

Mercury intrusion porosimeter (Micromeritics AutoPore® IV 9520, USA) was utilized to analyze the porosity and pore size of the three types of freeze-dried GGMA hydrogels. In brief, the porosimeter applies pressure (in psi) to fill the larger pores with mercury first, and as the pressure increases, the filling proceeds to smaller ones. The total volume of mercury intruded into the hydrogels (in cm^3) was then determined to assess the overall porosity and pore size. To further obtain more precise pore characteristics, cryo-fixed samples were analyzed through micro-computed tomography (micro-CT, SkyScan 1276, Bruker, USA). The sample preparation process is as follow. In brief, the sample is fixed with 3.7 % PFA (Paraformaldehyde) and OSO_4 to maintain its structural integrity. Subsequently, samples require vitrification. The vitrification method applied in GGMA-based hydrogels entails plunge freezing in liquid nitrogen to prevent the formation of water crystals. The rapid freezing step maintains hydrogel structures with greater fidelity compared to conventional freezing, enhancing the accuracy of data for assessing hydrogel pore size and porosity [52,53]. Next, process the sample using the critical point drying method (CPD, Hitachi HCP-2, Hitachi, Japan). Finally, the internal structure of hydrogels was then analyzed using micro-CT. This allowed assessment of the pore distribution, porosity, and size of the three types of GGMA-based hydrogels. Subsequently, the pores were colorized using image editing software to visualize the distribution and size of pores within the hydrogel.

2.8. Rheological test

To observe the gelation properties of GGMA-based hydrogels, analysis of hydrogel rheology was conducted. The rheological properties (storage modulus, G'; loss modulus, G") of GGMA-based hydrogels were obtained by stress-controlled Discovery Hybrid Rheometer HR-2 rheometer (TA Instruments, USA) with 20 mm parallel plate geometry and UV Light Guide accessory (TA Instruments, USA). Light intensity and wavelength of UV light source OmniCure® S2000 (Excelitas, USA) was fixed at 3.6 mW/cm^2 and 365 nm, respectively. All the experiment groups were conducted at room temperature with a strain of 1 %.

2.9. Thermogravimetric analysis (TGA)

Thermogravimetric analysis (TGA) was utilized to analyze the thermal decomposition profile for polymer components within GGMA-based hydrogels. The experiment was carried out from 20 °C to 700 °C under nitrogen purge (20 mL/min) in Thermogravimetric Analyzer (Pyris™ 1 TGA Thermogravimetric Analyzer, Perkin Elmer, USA). The lyophilized hydrogel samples (3 mg) were analyzed in a platinum pan at the heating rate of 10 °C/min.

2.10. Water uptake analysis

The water absorption capacity of the dry hydrogels was precisely assessed by measuring their weight in a buffer solution using a highly accurate analytical balance (ATX124, Shimadzu, Japan). To perform the evaluation, the dry hydrogels (W_0) were fully immersed in a PBS solution and carefully placed in a water bath maintained at a constant temperature of 37 °C. At specific time intervals (0, 0.5, 1, 2, 4, 8, 12, 24 h), the hydrogels were weighed with great precision to determine the exact rate at which it absorbed water. To ensure the utmost accuracy in the measurements, the wet hydrogels (W_1) at each time point were meticulously blotted using filter paper to eliminate any residual surface water, and its weight was meticulously recorded. The water uptake was calculated using the following formula:

$$\text{Water uptake W\%} = \frac{(W_1 - W_0)}{W_0} \times 100\%$$

2.11. Compressive mechanical property

The mechanical properties of the GGMA-based hydrogels were evaluated using Elastic Modulus Load Cells (LTS-200GA, Kyowa, USA). The samples had dimensions of 8 mm/8 mm/2 mm (L/W/H). Each hydrogel underwent compression at a rate of 6 mm/min to generate stress-strain curves. The test was terminated as the hydrogel fractured. Data obtained were analyzed, and the Young's modulus was calculated through the slope of stress-strain curve ranging from 5 to 10 strain%. Then, the mechanical properties of the hydrogel were assessed.

2.12. Degradation assay

In order to investigate the degradation behavior of the hydrogels, a series of experiments were conducted. Initially, the hydrogels were immersed in a phosphate-buffered saline (PBS) solution for a duration of 1 h. After a subsequent 24-h period of lyophilization, the hydrogels were carefully weighed, and the resulting weight was recorded as W_0. Subsequently, the hydrogels were submerged in Dulbecco's Modified Eagle Medium (DMEM/high glucose, Thermo Fisher, USA) supplemented with 10 % (v/v) Gibco fetal bovine serum (FBS, Thermo Fisher, USA),1 % (v/v) Penicillin-Streptomycin-Amphotericin B Solution (P/S/A, Biovision, USA), and 2.5 mg/mL of trypsin. The incubation was conducted over various time intervals: 0, 8, 16, 24, 32, 40, and 48 h, all maintained at a constant temperature of 37 °C. Upon completion of each incubation period, the hydrogels were subjected to lyophilization, and their weights were recorded as W_1. The *in vitro* remaining weight (W%) of the hydrogels was then calculated using the following formula:

$$\text{Remaining weight W\%} = \frac{(W_0 - W_1)}{W_0} \times 100\%$$

2.13. Murine fibroblast L929 cell

The L929 cell line was obtained from the Bioresource Collection and Research Centre (BCRC, Taiwan). The cells were cultured in high glucose DMEM (Dulbecco's Modified Eagle's Medium, HyClone, USA) supplemented with 10 % fetal bovine serum (FBS; Sigma-Aldrich, USA)

and 1 % antibiotic-antimycotic solution, which included 0.25 μg/mL amphotericin B, 75 U/ml penicillin, and 100 μg/mL streptomycin (Sigma-Aldrich, USA). Incubation occurred at 37 °C in a 5 % CO_2 humidified atmosphere.

2.14. Cell culturing and seeding for cytocompatibility in GGMA-based hydrogels

The cytocompatibility of GGMA-based hydrogels were assessed. Prior to cell seeding, all the hydrogels (diameter: 12.5 mm, thickness: 1.65 mm) underwent six rinses with PBS solution; the total cleaning session lasted for 6 min. The hydrogels were then immersed in culture medium (DMEM/F-12) at room temperature in 24-well culture plates for 1 h before seeding L929 cells (1×10^6/hydrogel) onto the hydrogels. Following a 6-h incubation at 37 °C with 5 % CO_2, the hydrogels were supplemented with 2 mL of complete medium. The culture medium was changed every 2 days.

2.15. Cell morphology and distribution in GGMA-based hydrogel

The L929 cells (1×10^6/hydrogel) cultured on GGMA-based hydrogels were stained with a phalloidin reagent (1:100 dilution, Invitrogen, USA) to evaluate their morphology under an inverted fluorescence microscope (Olympus, ix71, Japan). The GGMA-based hydrogels with the cells were cultured in a growth medium. After 1, 3, and 5 days of cultivation, the hydrogels were washed with PBS, fixed with 4 % paraformaldehyde in PBS for 15 min at room temperature, and rinsed three times with PBS to remove the fixative. Subsequently, the cells were permeabilized in PBS with 0.1 % Triton X-100. Each hydrogel was then immersed in 1 mL of PBS with a staining reagent for 1 h at 37 °C. Following the staining, the hydrogels were washed again, and the nuclei were stained with Hoechst 33342 (1:1000 dilution; Sigma-Aldrich, USA) for 5 min. Finally, the cell morphology images on the hydrogels were observed using a Leica TCS SP5 confocal microscope system (Zeiss, Oberkochen, Germany). The analysis of the cell images was performed using Leica LAS AF Lite.

2.16. Visualization of mitochondria in cells within GGMA-based hydrogels

To visualize the distribution of mitochondria in cells on GGMA-based hydrogels, L929 cells (1×10^6/hydrogel) were treated with MitoBright LT antibody (1:100 dilution; Dojindo, Japan) for 1 h prior to seeding them on the hydrogels. Following a 5-day cultivation period, the samples were subjected to three washes using PBS. The cells were then observed using a Leica TCS SP5 confocal microscope system and analyzed using Leica LAS AF Lite software. Finally, the fluorescent intensity of mitochondria of cells in each type of hydrogel was quantified using Image-J software.

2.17. Cell distribution and penetration depth in GGMA-based hydrogel

To track the distribution and penetration depth of L929 cells on GGMA-based hydrogels (diameter: 12.5 mm, thickness: 3.00 mm), L929 cells (1×10^6/hydrogel) were treated with MitoBright LT antibody (1:100 dilution; Dojindo, Japan) for 1 h prior to seeding them in the hydrogels. The samples were then observed using a BioTek Cytation 5 Cell Imaging Multimode Reader (Agilent Technologies, USA) during a 3-day cultivation period. Finally, the fluorescent intensity of mitochondria of cells in each type of hydrogel was quantified using BioTek Gen5 software. This quantification allowed us to estimate the cell migration within the hydrogels.

2.18. Cell viability in GGMA-based hydrogel

The L929 cells were first counted, and approximately 5×10^4/hydrogel were then seeded on GGMA-based hydrogels. Subsequently, the cells were incubated at 37 °C in a humidified atmosphere with 5 % CO_2 for 5 days, with the culture medium being replaced every two days. In this study, cell viability was quantified with CCK-8 assay kit (Merck, USA). At day 1, 3 and 5, the medium was removed, and the hydrogels were gently rinsed with PBS, followed by soaking in a mixed solution of 10 μL of CCK-8 reagent with 90 μL of culture medium at 37 °C for 3 h. The absorbance readings at a wavelength of 450 nm were observed using a multimode microplate reader (SpectraMax i3x, Molecular Devices, USA).

2.19. dsDNA assay

Cell proliferation within the GGMA-based hydrogels was assessed using the Quant-iT dsDNA assay (Invitrogen, USA). L929 cells (5×10^4/hydrogel) were cultured on the hydrogels for 1, 3, and 5 days, followed by washing the hydrogels with PBS solution. Subsequently, the hydrogels were immersed in TE buffer solution (200 mM Tris-HCL, 20 mM EDTA, pH 7.2) containing 0.5 % Triton X-100 (Sigma-Aldrich, USA) to facilitate cell lysis through three freeze-thaw cycles. The resulting lysate solution was then diluted with TE buffer and mixed with the PicoGreen reagent, following the manufacturer's instructions. Finally, the samples were subjected to analysis using a multimode microplate reader with excitation/emission wavelengths of 480/530 nm.

2.20. Cell proliferation and apoptosis of L929 cells within GGMA-based hydrogels were assessed using flow cytometry

Cell proliferation and apoptosis within GGMA-based hydrogels were assessed using the Muse® Ki67 Proliferation Kit (Luminex, USA) and the Muse™ Annexin V & Dead Cell Kit (Luminex, USA) through flow cytometry analysis. For intracellular staining, cells were collected and washed three times with ice-cold PBS following the manufacturer's protocol. Subsequently, the cells were suspended in 1× fixation solution and incubated at 4 °C for 20 min. After centrifugation and removal of the supernatant, the cells were washed three times with 1× assay buffer. Then, they were incubated with PE-conjugated monoclonal anti-Ki-67 antibodies at room temperature for 30 min. Flow cytometry analysis was performed using the Guava® Muse Cell Analyzer (Luminex, USA) with Muse Cell Analyzer software for data acquisition and analysis. To investigate cell apoptosis in GGMA-based hydrogels, flow cytometry analysis was conducted using Annexin V-PE/7-AAD staining. Cells were collected and rinsed three times with ice-cold PBS. Next, the cells were washed and incubated with Annexin V-PE/7-AAD reagent (Luminex, USA) for 20 min at room temperature. The cells were then analyzed using the Guava® Muse Cell Analyzer with Muse Cell Analyzer software for data acquisition and analysis. Flow cytometry collected 1×10^5 cells from all samples analyzed.

2.21. Adhesion testing of hydrogels on mouse tissue organs

To assess the tissue adhesion strength of GGMA-based hydrogels, a mold was first placed on a glass slide. Subsequently, 100 μL of hydrogel was added to the mold, followed by cross-linking with UV light at the wavelength of 365 nm. The mold was then removed, and the hearts, livers, kidneys, and spleens of mice were placed on the hydrogel, with organs lightly pressed and secured using forceps. Finally, the glass slide was inverted to observe the adhesion of the organs to the hydrogel, and photographs were taken for documentation.

2.22. Adhesion test of hydrogels on porcine skin

To assess the tissue adhesion strength of hydrogels quantitatively, we conducted two lap-shear adhesion tests following ASTM F2255-05 guidelines, albeit with some adjustments. Initially, we obtained 1 cm × 2 cm squares from porcine skin tissue and adhered them to two glass

slides using cyanoacrylate glue. Subsequently, we applied 100 μL of GGMA-based hydrogel between the two skin tissues in situ, followed by polymerization under 365 nm UV irradiation for 1 min. Each assembly was then subjected to a 2500 g weight for 1 h. Finally, the lap-shear strengths of the samples were measured using a texture analyzer (A. XTplusC Texture Analyser, Stable Micro Systems, USA) at a tracking speed of 0.1 mm s^{-1} (Fig. 4C and D).

2.23. Hemostatic capacity of GGMA-based hydrogels in liver tissue

To assess the hemostatic potential of the GGMA-based hydrogels, we utilized a hemorrhaging mouse liver model. The Institutional Animal Care and Use Committees (IACUC) of the Taipei Medical University approved the animal care guidelines. The mice were anesthetized using 4–5% Isoflurane gas in an Induction Chamber. Once they reached a light anesthesia stage, they were carefully positioned on a surgery board with their abdomen facing upwards. To maintain a deep anesthesia state, 1–3% Isoflurane was continuously administered through a face mask. Subsequently, the mouse experiment commenced. After making an abdominal incision, medical grade paper was used to wipe the serous fluid around the liver. A pre-weighed filter paper on a paraffin film was placed beneath the liver. We induced bleeding from the liver using a 25G needle to puncture and immediately applied 100 μL of GGMA-based hydrogel solution to the site of bleeding. The hydrogel was cross-linked by UV-light irradiation for 30 s, and recorded the time it took for the liver tissue to stop bleeding after bleeding started. Afterward, observed and photographed the adhesion of the hydrogel to the liver tissue. Finally, the weight of the filter paper was measured to assess the amount of bleeding from the liver.

2.24. Full-thickness skin wound model

Male ICR (CD1) mice weighing 24.2–26.6 g were selected for the animal wound healing experiment. The mice, provided by the National Laboratory Animal Center (Taipei, Taiwan), were treated following the animal care guidelines of Taipei Medical University. For the skin wound model, the dorsal hair of the mice was removed after administering Zoletil (Zoletil 50, Virba, Taiwan) for paralysis. A circular skin tissue on the back of the mice was then excised using a sterile biopsy punch to create a full-thickness excisional wound with a diameter of 2 cm. To prevent wound infection, Mitomycin C solution (1.5 mg/kg) was applied to the surrounding area. The mice were divided into four groups for the skin wound healing model: the wound treated with GGMA, GGMA/HK, GGMA/FK, and a control group treated with PBS. The hydrogels directly covered the wound area, and the dressing was changed every 2 days. During the hydrogel dressing change, wound healing was observed and photographed using a dissecting microscope photography system (SZ61 Stereo Microscope, Olympus, Japan). Afterward, the ImageJ software system was utilized to visualize the wound area and quantify wound contraction, providing an objective assessment of healing progress. On the 17th day post-wounding, all mice in the groups were euthanized using CO_2 inhalation. The repaired skin tissue, along with a margin of surrounding skin, was harvested from each group of mice. The tissues were fixed in 10 % formaldehyde (Sigma-Aldrich, USA), embedded in paraffin, sectioned, and stained with hematoxylin and eosin staining kit (H&E staining kit, Abcam, USA) and Masson's trichrome staining kit (Merck, USA) for in *vivo* evaluation of epidermal wound healing and perilesional tissue fibrosis in mice. Simultaneously, immunohistochemistry CD31 staining (diluted at 1:100; Millipore, USA) was employed to assess angiogenesis in the wound healing process. All staining procedures were conducted according to the manufacturer's provided protocols.

2.25. Statistical analysis

The data are presented as means with standard deviations (SD). GraphPad Prism 8.3 software was utilized for comparing different groups using either one-way analysis of variance (ANOVA) or the Student's t-test. Statistical significance was defined as $^{*}p < 0.05$, $^{**}p < 0.01$ and $^{***}p < 0.001$.

3. Results and discussion

3.1. Synthesis of GGMA-based hydrogels

Prior to fabricating the hydrogel, SDS-PAGE analysis was employed to confirm the extracted proteins from hair and feather roots as keratin (Fig. S1A). The keratin extracted from hair exhibited heterogeneity, with a molecular weight range of approximately from 25 to 75 kDa. Furthermore, SDS-PAGE revealed the presence of keratin-associated proteins (KAPs; <20 kDa) in the hair samples. In the case of feather keratin, smaller molecular weight proteins were observed, with fragment sizes approximately within the range from 10 to 17 kDa. This observation is consistent with previous research and confirms the accurate extraction of keratin from both species. From CD spectrum result (Fig. S1B), we can observe that hair keratin exhibit mainly alpha-helix structure with slight amount of beta-sheet within. As for feather keratin, the structure represents the combination of random coil and beta-sheet. This finding also corresponds with previous literature [54]. For amino acid analysis result (Fig. S1C), we can find the amino acid compositions between hair and feather keratin are slightly different, which might be caused by the difference in extraction method. However, the trends of amino acid composition are similar to results conducted from previous literature [55,56]. Higher composition of Asp, Arg and Lys could lead to higher possibility in forming cell adhesion motif (i.e. RGD sequence) to promote cell adhesion [57]. Therefore, we believe that the incorporation of hair keratin into GGMA would exhibits better performance in cell adhesion tests than the group containing feather keratin.

In the preparation process, methacrylic acid (MA) was effectively grafted onto gellan gum molecules, with the proportions finely adjusted based on successful methods from previous studies [50] (Fig. 1). The resulting hydrogels—GGMA, GGMA-Human hair keratin (GGMA/HK), and GGMA-Feather keratin (GGMA/FK)—were synthesized through photo-crosslinking. The distinct appearances of each hydrogel, illustrated in Fig. 1, reflect differences due to the inclusion or exclusion of keratin and the use of different keratin types. Beyond visual differences, variations in internal molecular structures and crosslinking conditions among the hydrogels may exist and were subsequently investigated to evaluate their chemical and physical properties.

The incorporation of feather keratin (FK) and hair keratin (HK) into gellan gum methacrylate (GGMA) hydrogel, respectively, were verified through FT-IR and ^{13}C NMR. In Fourier transform infrared spectroscopy (FT-IR) analysis, several distinctive bands can be observed, each providing valuable information about the molecular constituents present in the samples (Fig. 2A). ^{13}C nuclear magnetic resonance (NMR) spectroscopy analysis revealed specific peaks indicative of distinct functional groups within the material under investigation (Fig. 2B). Through comparing and analyzing the results of FT-IR and ^{13}C NMR on GGMA, HK, FK, GGMA/HK, and GGMA/FK, we can confirm the existence of keratin within the hydrogels.

3.2. Structural analysis of GGMA-based hydrogels

Appropriate pore size and porosity of hydrogels promote cell proliferation and differentiation by facilitating the delivery of essential substances. Therefore, this study investigates the internal characteristics of three GGMA-based hydrogels (GGMA, GGMA/HK, and GGMA/FK).

The SEM images reveal the internal structures of the freeze-dried hydrogels based on GGMA, GGMA/HK, and GGMA/FK (Fig. S2). Upon examining the hydrogel structures, the cross-sectional images show that three hydrogels have comparable internal structures, consisting of extensive interwoven mesh-like formations that contain numerous

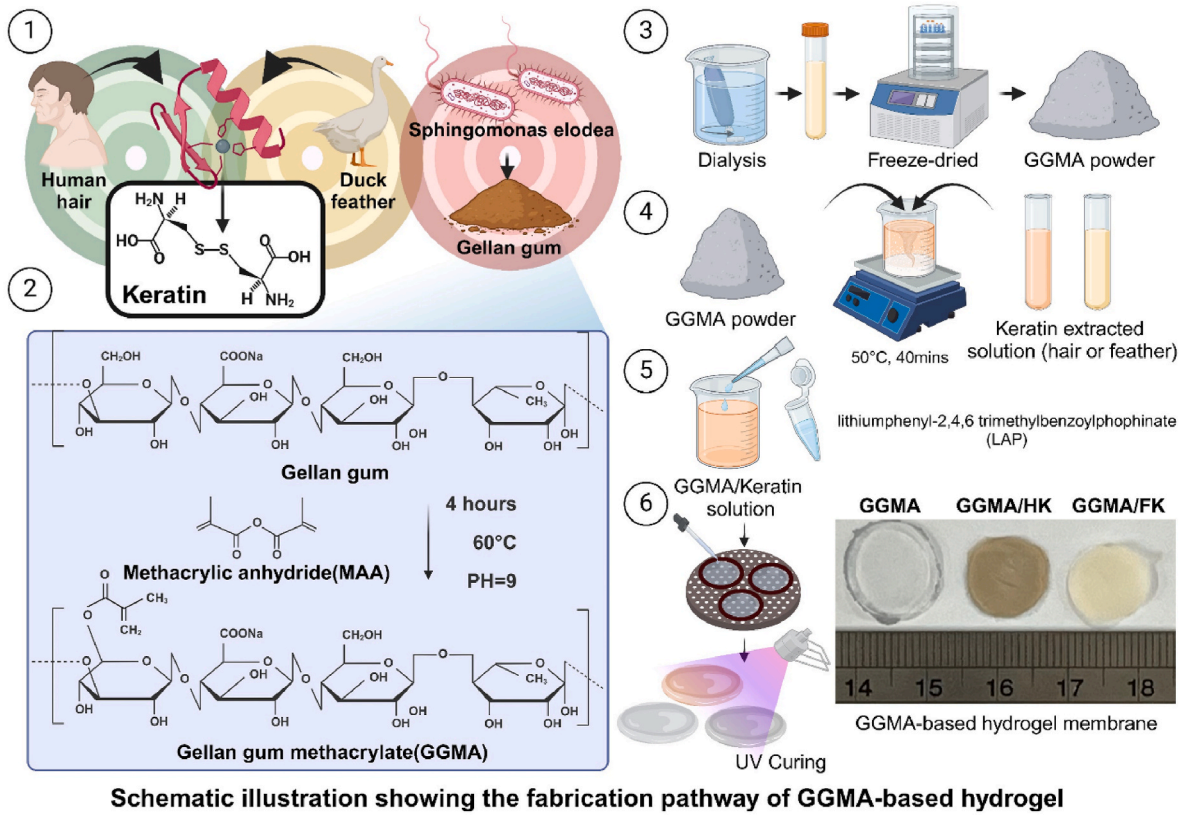

Fig. 1. A graphical representation depicting several steps: preparation of the materials needed for GGMA-based hydrogels, synthesis and hydrogel preparation process, formation of GGMA molecules through a chemical reaction between gellan gum and methacrylic anhydride (MAA), fabrication of GGMA (transparent), GGMA/HK (pale brown), and GGMA/FK (light ivory) hydrogels, and the appearance of the structures for these three types of hydrogels arranged from left to right.

pores. Interestingly, differences were observed in the structure between the GGMA/HK and GGMA/FK groups, suggesting that the incorporation of keratin from different sources results in distinct structural characteristics.

Mercury intrusion porosimetry (MIP) analysis was used to assess the average pore sizes, the quantifications are as follow: 128.5 ± 3.5 μm for GGMA, 110.2 ± 7.2 μm for GGMA/HK, and 159.3 ± 2.9 μm for GGMA/FK (Table 1). It was observed that in the GGMA-based hydrogel group with feather-extracted keratin, the average pore size was the largest. However, in the GGMA/HK group, the average pore size was the smallest among these three types of hydrogels. Meanwhile, the porosity of these three hydrogels was determined to be 87.58 % for GGMA, 82.46 % for GGMA/HK, and 77.54 % for GGMA/FK (Table 1). Based on this data analysis, the effective porosity of these three hydrogels can be ranked as follows: GGMA > GGMA/HK > GGMA/FK. Previous research indicates that various cell types require different pore sizes for optimal survival, with sizes generally beginning at approximately 50 μm [58]. Although the actual internal pore size of these hydrogels may be smaller than what is obtained, due to formation of water crystals in sample preparation, through mercury intrusion porosimetry, we speculate that all three types of hydrogels should still have sufficient internal space to provide an appropriate microenvironment, however, further investigation is needed.

In order to obtain precise information about the pore structure of the GGMA-based hydrogel by directly visualizing and quantifying the pore distribution and size, micro-CT was employed on cryo-fixed hydrogel samples. The pore characteristics observed from micro-CT are likely to be more accurate, as the formation of water crystals, which could alter hydrogel structures during the preparation process, was minimized. Meanwhile, this system, equipped with colorization software, visualized the internal structures of the hydrogels and quantified their overall porosity. By using different colors to distinguish the sizes of internal pores in the gel, one can closely observe the distribution and dimensions of water molecule pores. This integrated approach enables a more comprehensive understanding of the hydrogel's microstructure (Fig. 2C).

Through quantitative analysis, the pore sizes and porosities for the three hydrogels are as follows: 63.36 ± 3.1 μm, 80.28 % for GGMA; 60.12 ± 1.8 μm, 78.82 % for GGMA/HK; 51.71 ± 2.5 μm, 73.47 % for GGMA/FK (Table 1). Based on this data analysis, the pore sizes and effective porosities of these three types of hydrogels can be ranked as follows: GGMA > GGMA/HK > GGMA/FK. Based on the micro-CT analysis, all three types of hydrogels should provide adequate permeability during cell culture, suggesting that GGMA-based hydrogels offer sufficient space for cell survival. A series of cell compatibility experiments will be conducted to test whether cells can maintain normal cellular functions within these hydrogels.

3.3. *Versatile physical properties of GGMA-based hydrogels*

In development of hydrogels, previous studies have adjusted their structures and properties with various preparation processes [49,59,60]. Therefore, evaluation of GGMA-based hydrogels on their water absorbency, mechanical performance, and material degradation is conducted.

To investigate the photo-crosslinking gelation properties of GGMA-based hydrogels, the rheological test with ultra-violet (UV) curing was conducted. As shown in Fig. 2D, we could observe that the storage modulus (G′) of all hydrogel groups drastically increased as the UV light source was activated at the 30th second of the test time, while the loss modulus (G″) also slightly increased. Furthermore, we could notice that the values of G′ in all groups were obviously higher than that of G" and stabilized at the 100th second of test time. This result indicates that the hydrogels possess rapid gelation properties under UV curing which would be helpful to the further tests. Also, we could find that the

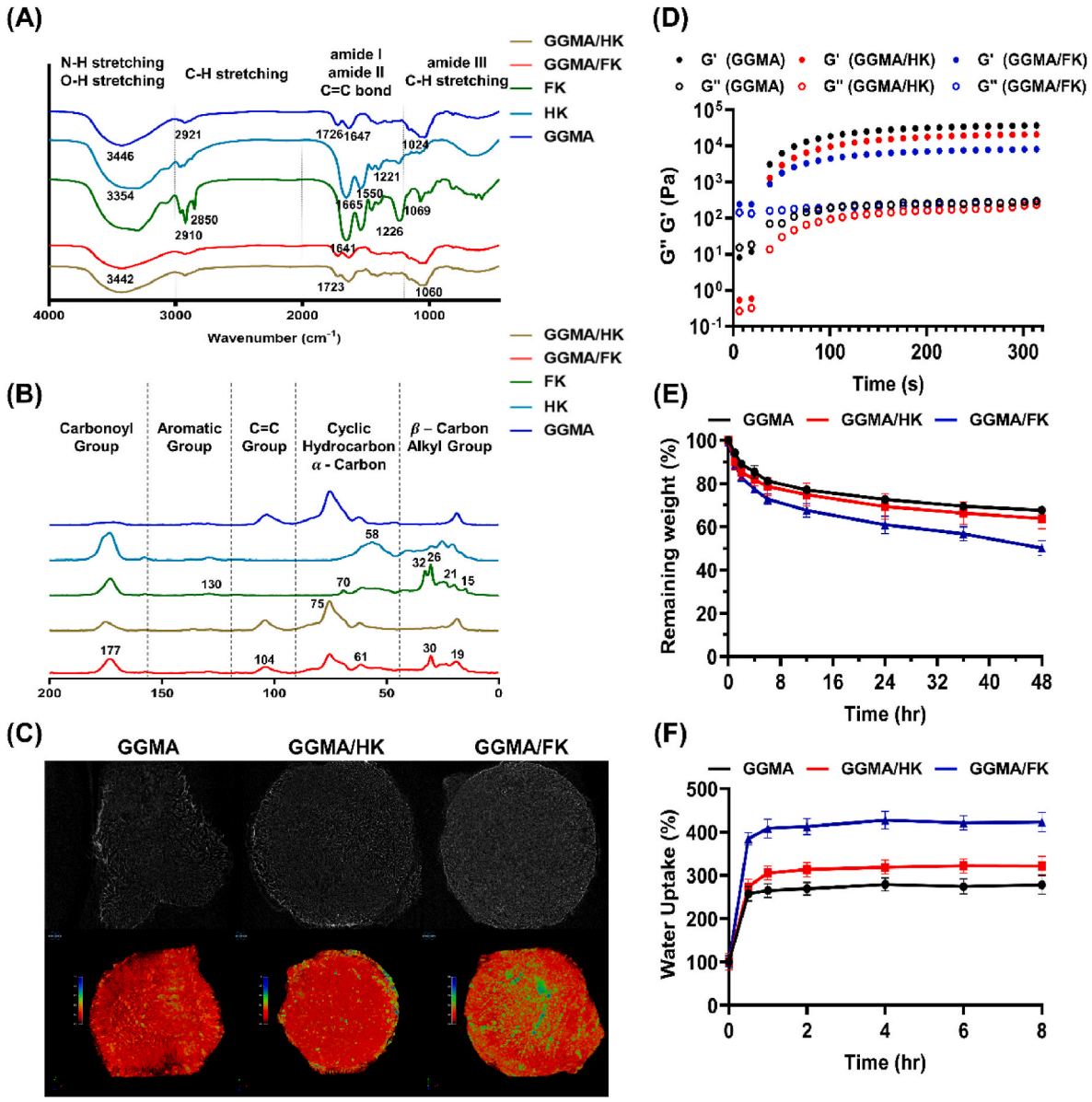

Fig. 2. Physical property analysis of GGMA, GGMA/FK, and GGMA/FK hydrogels. (A) Utilization of FT-IR analysis to examine the functional groups within three GGMA-based hydrogels and the necessary constituents (feather, hair keratin) (B) Using ^{13}C NMR instrumentation, the molecular compositions within three GGMA-based hydrogels and the essential source materials (feather, hair keratin) are analyzed to identify their molecular functional groups. (C) Micro-CT image for pore distribution within GGMA-based hydrogels. (D) Rheological measurement of GGMA-based hydrogels with 365 nm UV-light curing. (n = 3) (E) Evaluation of the *in vitro* degradation of GGMA-based hydrogels over a 48-h period. (n = 3) (F) Measurement of the water uptake of three types of hydrogels within 8 h (n = 3).

Table 1
Pore sizes and porosities of GGMA hydrogels analyzed with mercury intrusion porosimetry (MIP).

	GGMA	GGMA/HK	GGMA/FK
Pore size (MIP)	128.5 ± 3.5 μm	110.2 ± 7.2 μm	159.3 ± 2.9 μm
Pore size (micro-CT)	63.36 ± 3.1 μm	60.12 ± 1.8 μm	51.71 ± 2.5 μm
Porosity (MIP)	87.58 %	82.46 %	77.54 %
Porosity (micro-CT)	80.28 %	78.82 %	73.47 %

incorporation of keratin would slightly affect the cross-linking process of GGMA hydrogels as the values of G′ in both groups with keratin content were slightly lower than that of the GGMA group. As for the difference between GGMA/HK and GGMA/FK groups in G' values, this might be caused by differences in crosslinking efficiency between hair and feather keratin.

From Fig. 2D, we investigate different time point at which each hydrogel reached the same value of storage modulus (Fig. S3A). We assume that the networks within the hydrogels are composed entirely of GGMA polymers, as keratin does not contain functional groups to crosslink with GGMA polymers. Consequently, if two hydrogels achieve the same storage modulus, implying that they have reached equivalent crosslinking densities. By measuring the time required for each hydrogel to attain this specific density, we can compare their crosslinking efficiencies, GGMA > GGMA/HK > GGMA/FK. The main distinction between these hydrogels, influencing their crosslinking efficiency, should be the incorporation of keratins. Since the molecular weight distribution for the extracted feather keratin is relatively smaller than that of hair keratin, there is more polymer chains within the hydrogel than that of hair keratins, causing the crosslinking possibility between C–C double bonds of GGMA polymers to be relatively lower for GGMA/FK group than GGMA/HK group, resulting in lower G' values. However, the result

of the rheological test still proved that GGMA polymer could retain sufficient gelation properties after the incorporation of hair and feather keratin.

In the degradation test, we can observe that the remaining weight of all groups of hydrogels are above 60 % after 48 h (Fig. 2E). We can also find that the GGMA and GGMA/HK groups show similar trends during the test time. However, the remaining weight of the GGMA/FK group is relatively smaller than the other groups and this result might be caused by lower crosslinking density, making it easier to degrade.

According to the experimental results of water absorption test, the three types of hydrogels reached water absorption equilibrium at approximately 1 h. Further evaluation of their water absorption capacity revealed the following order: GGMA/FK > GGMA/HK > GGMA (Fig. 2F). Although GGMA hydrogel itself possesses some water absorption potential, its water uptake is still inferior compared to the hydrogels with added keratin. The superior water absorption of GGMA/FK can be attributed to the hydrophilic groups, which facilitate water molecule adsorption and penetration. Additionally, using an alkaline method for extracting feather keratin resulted in the cleavage of keratin into smaller molecule β-keratin derivatives, leading to an increased exposure of hydrophilic groups such as amino and sulfhydryl groups. This enhanced the water absorption ability of GGMA/FK hydrogel. On the other hand, GGMA/HK exhibiting lower water absorption compared to GGMA/FK due to the hair keratin extraction method using 2-mercaptoethanol and heat, resulting in longer molecular chains with fewer exposed hydrophilic groups. Our findings demonstrate that the addition of keratin significantly impacts the water absorption properties of the hydrogels, and the extent of exposure of hydrophilic groups during the keratin extraction process may be a critical factor contributing to the differences in water absorption.

According to previous literature, the mechanical strength characteristics of materials containing keratin are generally poor, mainly due to the hard and brittle nature of keratin proteins [36]. Since GGMA possesses excellent mechanical properties, we introduced GGMA to provide structural support to keratin. From the result of the compression test, we observed that the Young's modulus of these three hydrogels follows the order of GGMA > GGMA/HK > GGMA/FK (Fig. S3B). We could observe that the incorporation of keratin would slightly affect the mechanical property of GGMA hydrogel. Interestingly, we could also notice that GGMA/HK possess higher value in Young's modulus than that of GGMA/FK. One possible reason may lie in the difference of size distribution between two extracting methods of keratins. Hair keratins contain higher content of flexible α-keratin secondary structures. On the other hand, due to the utilization of strong alkali during the extraction process, the β-sheet structures of feather keratin might be degraded into small molecule β-keratin derivatives. Their respective interference with the crosslinking between GGMA polymers led to a lower mechanical strength of GGMA/keratin hydrogels compared to GGMA. Nevertheless, with the slight difference in Young's modulus, the mechanical characteristics of GGMA network were not adversely affected by the incorporation of keratin, proving GGMA to be effective in providing mechanical support for the keratin content.

From the TGA results (Fig. S3C), we can know that there exist three different temperature ranges of thermal decomposition. The first temperature range of decomposition is 0–100 $^{\circ}C$ and the weight loss is mainly due to the evaporation of remaining water inside the material. The second range of thermal decomposition happens around 250 $^{\circ}C$ and the weight loss is mainly due to the decomposition of GGMA which we can observe in all hydrogel groups. The final temperature range of decomposition is 300–320 $^{\circ}C$, mainly caused by the decomposition of the keratin component which is observed in the both groups containing keratin. Interestingly, we can observe that the decomposition temperature of GGMA in the GGMA/FK group is relatively lower than the other groups. The phenomenon might be caused by the interaction of feather keratin with GGMA hydrogel which we can also notice from rheological property, compressive test and degradation assay. The final remaining weight % of both GGMA/keratin groups is relatively larger than that of the GGMA group, this might be caused by the keratin remains and impurities produced from the extracting process. In spite of the slight change in degradation temperature of hydrogel groups containing keratin, the incorporation of keratin would not significantly affect thermal decomposition profile of GGMA hydrogels.

In summary, these results provided an insight into the physical characteristics of GGMA/keratin hydrogel. With this understanding of GGMA/keratin hydrogels, we then conducted a series of *in vitro* and *in vivo* experiments to analyze the applicability of GGMA/keratin hydrogels.

3.4. Cell localization, viability and proliferation throughout the GGMA-based hydrogels

To assess cellular behavior within GGMA-based hydrogels, L929 cells were cultured for 5 days, fixed, and stained with phalloidin for filamentous actin and MitoBright LT for mitochondrial distribution. Confocal microscopy showed strong phalloidin and MitoBright LT expression in GGMA/HK and GGMA/FK groups compared to GGMA alone (Fig. 3A, S4A).

The cells predominantly display spindle or spread-out morphologies, with the staining signals and quantification of phalloidin expression stronger in GGMA/HK and GGMA/FK groups compared to GGMA throughout the study (Fig. 3A, S4B). W hile GGMA/HK exhibits slightly higher staining than GGMA/FK with no significant difference.

On day 5, mitochondrial expression also revealed cell morphology within GGMA-based hydrogels, corresponding to the spindle-shaped morphology observed in previous result. Both GGMA/HK and GGMA/FK groups exhibited significantly higher staining signal levels compared to GGMA (Fig. S4A). Also, quantification result showed the same trends, with GGMA/HK showing notably higher levels on days 3 and 5 (Fig. S4C). From the results, it is evident that the interior of GGMA/keratin hydrogels can foster favorable conditions for cell adhesion, with GGMA/HK demonstrating a particularly enhanced cell attachment environment.

Next, we assessed L929 cell viability and proliferation within GGMA, GGMA/HK, and GGMA/FK hydrogels using CCK-8 assay, dsDNA content, and Ki-67 expression from day 1 to day 5. CCK-8 assay revealed increasing metabolic activity in all groups throughout the experiment period. Initially, GGMA/HK and GGMA/FK groups showed higher formazan products expression than GGMA, with GGMA/HK slightly higher than GGMA/FK (Fig. 3B). At days 3 and 5, GGMA/HK displayed significantly higher activity than GGMA/FK, while GGMA presented lowest activity level, likely due to the absence of keratin. Despite this, cell viability tests continue to demonstrate that all GGMA-based hydrogels are highly compatible with cells.

The dsDNA assay detected cell proliferation in the hydrogel (Fig. 3C). In all groups, dsDNA concentration increased from day 1 to day 5, with the GGMA/HK group showing the highest increment. On day 5, both GGMA/HK and GGMA/FK groups had significantly higher dsDNA concentrations than the GGMA group, with GGMA/HK exhibiting the highest concentration, indicating that it is conducive for cell activity and enhancing L929 cell proliferation within GGMA-based hydrogels containing keratin.

To assess cell proliferation in GGMA-based hydrogel, we analyzed Ki-67 expression. Ki-67, encoded by the human MKI67 gene, is predominantly expressed during active cell cycle phases (G1, S, G2, and M), making it a common marker for assessing proliferation [61].

Based on flow cytometry, Ki-67 expression in GGMA, GGMA/HK, and GGMA/FK groups on day 1 was 16.91 %, 31.02 %, and 21.47 %, respectively (Fig. 3D). On day 5, expression increased: GGMA (27.29 %), GGMA/HK (73.44 %), and GGMA/FK (67.15 %). Keratin-containing hydrogels showed significant increase in cell proliferation from day 1–5, with GGMA/HK showing the highest increment (Fig. 4D). Also, quantitative analysis (Fig. 3E) confirmed GGMA/Keratin hydrogels'

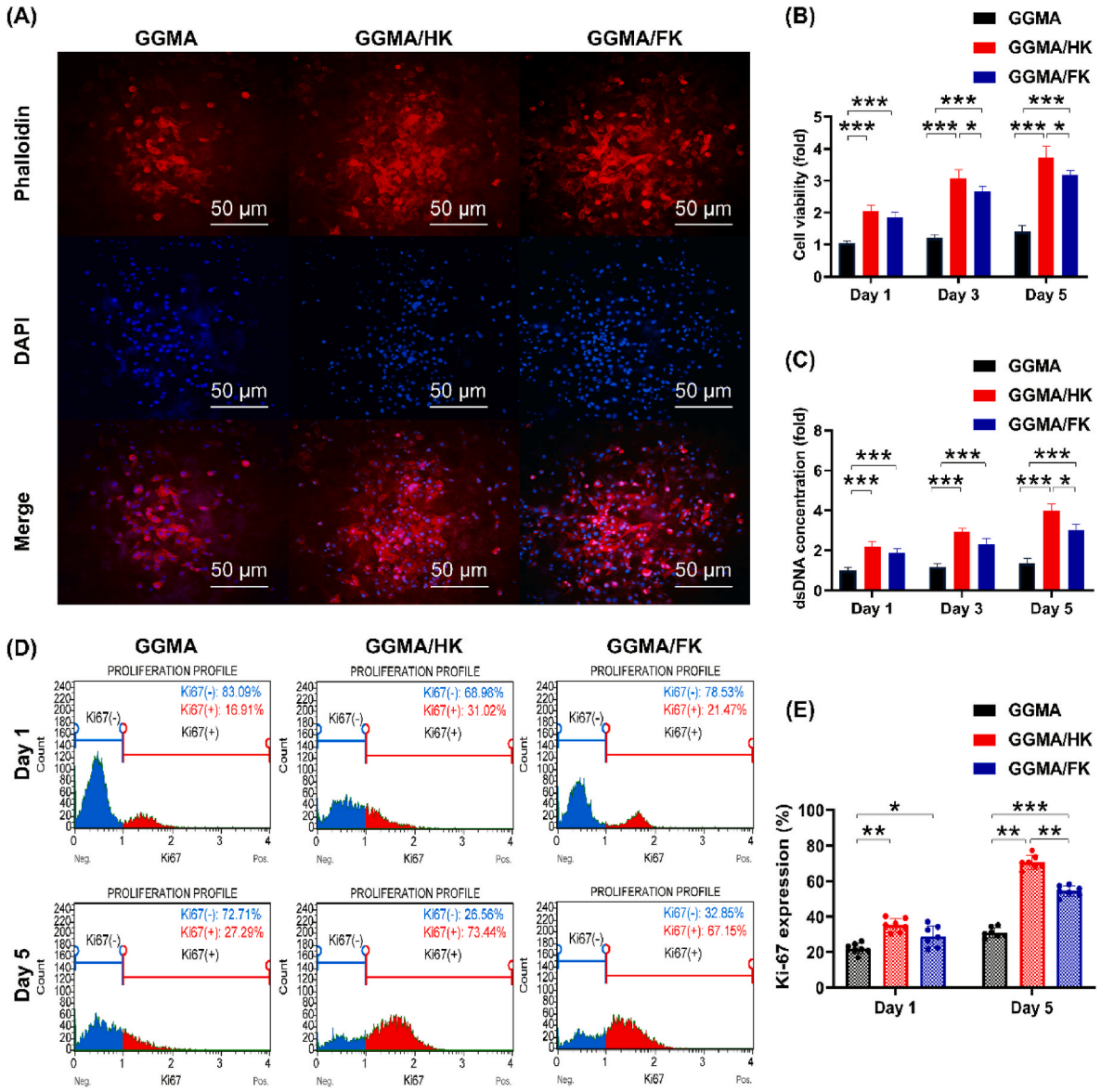

Fig. 3. Investigation of the cell compatibility and proliferation of L929 cells within hydrogel structures of GGMA, GGMA/HK, and GGMA/FK. (A) Utilizing phalloidin staining, the adhesion and distribution of L929 cells within GGMA, GGMA/HK, and GGMA/FK hydrogels are examined on day 5. (B, C) Quantitative analysis of Formazan production using the CCK-8 assay and measurement of DNA content were performed to assess the cell viability and proliferation of L929 cells within the GGMA, GGMA/HK, and GGMA/FK hydrogels at day 1, 3, and 5. (n = 6) (D, E) The scheme employed for flow cytometry analysis of cell proliferation and Ki67 expression in L929 cells derived from GGMA, GGMA/HK, and GGMA/FK hydrogels. Quantitative analysis of Ki67 expression was conducted on the three groups of hydrogels at day 1 and 5. (n = 6) *$p < 0.05$. **$p < 0.01$. ***$p < 0.001$.

superior performance over GGMA. This aligns with CCK-8 and dsDNA assay results. Differences may stem from variations in RGD (arginine-glycine-aspartate) and LDV (leucine-aspartate-valine) amino acid sequences in keratin extraction methods [57]. Nonetheless, keratin-enriched GGMA hydrogels effectively promote cell adhesion and proliferation, indicating excellent biocompatibility.

3.5. Assessment of cell apoptosis within GGMA-based hydrogels

The microenvironment of hydrogels impacts cell behaviors throughout their lifecycle, including diffusion, migration, proliferation, and apoptosis. To analyze these effects, we employed flow cytometric analysis on three types of GGMA hydrogels with L929 cells (Fig. S5). Flow cytometry quadrant analysis demonstrates the distribution of viable (7AAD-, Annexin V-), early apoptotic (7AAD-, Annexin V+), late apoptotic (7AAD+, Annexin V+), and dead (7AAD+, Annexin V-) cells.

On day 1, GGMA/HK and GGMA/FK groups exhibited over 98 % viability, with less than 1 % in late apoptosis or dead stages, indicating high cell compatibility (Fig. S5A). In contrast, GGMA showed 84 % viability, with 18.7 % in early apoptosis. Quantitative data from four experiments showed significantly higher viability in GGMA/HK and GGMA/FK groups (GGMA/HK: 97.56 %, GGMA/FK: 97.39 %) compared to GGMA (82.26 %), with no significant apoptosis observed in GGMA/HK and GGMA/FK groups. On day 5, GGMA/HK and GGMA/FK groups maintained high viability (96 %), while the viability of GGMA decreased to 70 %, with increased early apoptosis (28.72 %). Despite a slight increase in early apoptosis in GGMA/HK and GGMA/FK groups, the overall result exhibited high viability (Fig. S5B). In contrast, GGMA showed a significant decrease in viability (72.86 %) and increase level in early apoptosis (26.53 %) compared to day 1. This suggests that GGMA/keratin hydrogels provide a suitable microenvironment for prolonged cell growth, with GGMA alone showing reduced viability over time due

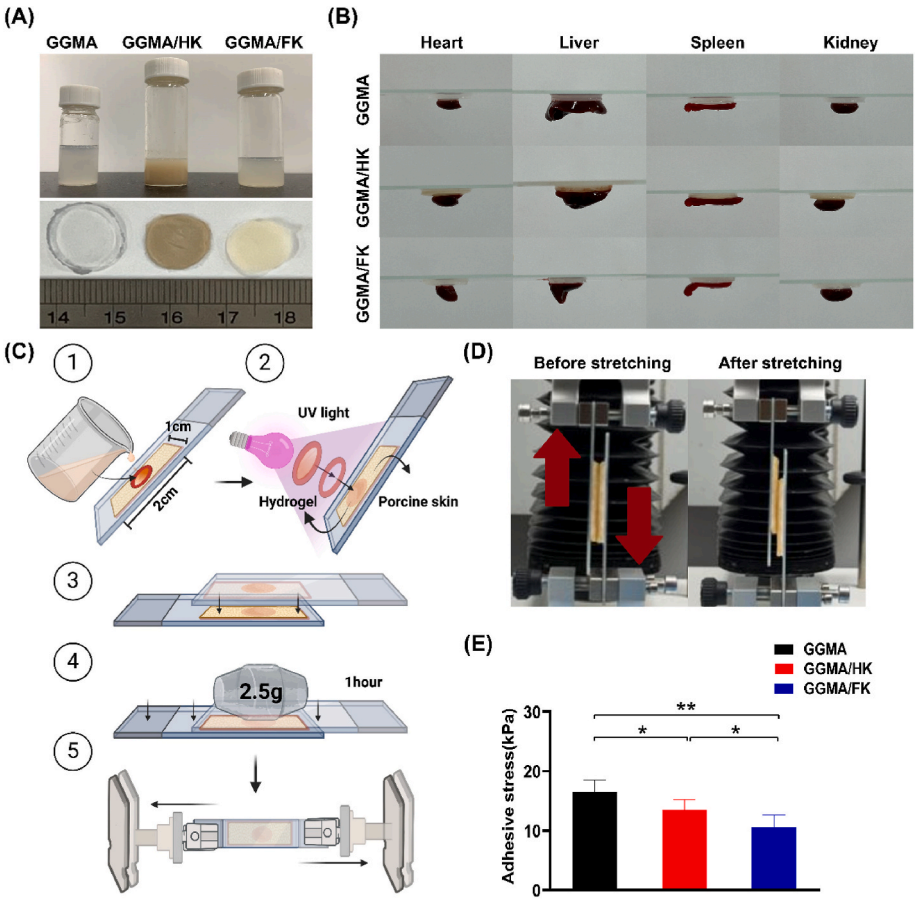

Fig. 4. Tissue adhesive properties of (A) GGMA, GGMA/HK, and GGMA/FK hydrogels appear as a liquid appearance before UV crosslinking and transform into a gel state after photo polymerization process. (B) Photos showing the adhesion ability of GGMA, GGMA/HK, and GGMA/FK hydrogels for the heart, liver, spleen, and kidney of mice. (C, D) Schematic illustration of the prepared sample and lap shear test, as well as the actual stretching condition of the samples. (E) Evaluation of the shear adhesion strength of GGMA, GGMA/HK, and GGMA/FK hydrogels. (n = 4) $*p < 0.05$. $**p < 0.01$.

to the absence of keratin as an adhesion substrate.

3.6. Observation of cell migration within GGMA-based hydrogels

To visualize live cell migration within the hydrogels, we utilized Cytation 5 combined with automated microscopy to obtain fluorescence images, as shown in Fig. S6. While the majority of the cells were observed to remain in the top section of the hydrogel after 24 h, they exhibited deeper migration into the hydrogel over a 72-h period (Fig. S6A, Fig. S7). In the case of GGMA/HK and GGMA/FK groups, we noticed that cells had penetrated approximately 2500 μm into the hydrogel. On the contrary, when observing the GGMA group at the same time point, most cells were confined to a specific section within the hydrogel, with cell positions ranging from approximately 450 to 1200 μm.

By quantifying the fluorescence-based movement of live cells, we calculated the migration distance of cells within the three types of hydrogels. As shown in Fig. S6B, the cell migration distances in different hydrogels were 2535 μm (GGMA/HK), 2591 μm (GGMA/FK), and 1145 μm (GGMA), respectively. Despite the GGMA hydrogel having a similar porous structure to GGMA/HK and GGMA/FK hydrogels, difficulties persisted in the process of cell migration within the GGMA hydrogel.

This phenomenon could be attributed to the enriched keratin protein content within both GGMA/HK and GGMA/FK hydrogels. These hydrogels not only exhibit a dense porous structure with appropriate pore sizes, allowing for the smooth flow of cell-containing culture medium, but also contain proteins within, serving as a substrate for cell adhesion and migration. Consequently, viable cells can effectively migrate and proliferate within the hydrogel. The results are in line with the study conducted by Ng KW et al., which underscores the effectiveness of keratin hydrogels in promoting fibroblast cell adhesion, proliferation, and maintaining cell viability [62]. These findings suggest that GGMA/keratin hydrogels, abundant in keratin protein, facilitate cell migration and adhesion.

3.7. Assessing the adhesive properties, strength, and hemostatic potential of GGMA-based hydrogels on biological tissues

To assess the adhesive effect of GGMA-based hydrogels on biological tissues, we conducted separate tests with plain hydrogels and photo-crosslinking to evaluate the adhesion of the GGMA-based hydrogels on different tissues (Fig. 4A). When organs were placed on the hydrogel and observed upside down, the GGMA-based hydrogels exhibited excellent adhesive performance to various biological tissues, including the heart, kidney, spleen, and liver, highlighting their importance for biomedical applications (Fig. 4B). Additionally, two lap-shear samples were prepared and the adhesion strength of the hydrogel on representative surfaces was determined using a tensile adhesion test (Fig. 4C and D). The adhesion stress to GGMA, GGMA/HK, and GGMA/FK was quantified as 16.5 ± 2.03, 13.5 ± 1.69, and 10.6 ± 2.06 kPa, respectively, through the tensile adhesion test (Fig. 4E). Although the keratin content may have slightly affected the crosslinking efficiency of GGMA hydrogel, thereby influencing its adhesive strength, GGMA/HK and GGMA/FK hydrogels still demonstrated a considerable degree of adhesiveness in

the tests.

Next, in order to verify the applicability of GGMA-based hydrogels in the cases of acute trauma, *in vivo* tests for hemostatic capacity were conducted on a mouse liver injury model (Fig. 5A). Fig. 5B shows the blood loss conditions for each group on filter paper, while the liver tissue images of hydrogel seals at the wounded site of liver tissue after being punctured. We could observe that, without hydrogels, the amount of blood loss was higher than the groups with hydrogels. Additionally, we could find that the hydrogel liquid forms a protective layer (red arrows) after photo-crosslinking, effectively isolating the wound from external contact thereby achieving hemostasis rapidly (Fig. 5B). Next, the quantified blood loss (Fig. 5C) revealed that the average bleeding amount during puncture was 27.8 ± 5.77 mg, 17.7 ± 6.0 mg, 14.5 ± 3.14 mg, and 15.3 ± 2.98 mg, respectively. The quantified hemostasis time (Fig. 5D) revealed that the average duration was 142.3 ± 29.51 s without using hydrogels, 37.6 ± 6.06 s for the GGMA group, 44.2 ± 7.12 s for the GGMA/HK group, and 44.3 ± 8.15 s for the GGMA/FK group. Overall, the groups with hydrogel covered exhibited significantly lower bleeding amounts compared to the control group. Furthermore, when comparing the effects of the three types of hydrogels on liver bleeding, no significant differences in bleeding time or blood loss were observed among three groups. This is because the hydrogels could directly fill the wound and physically isolate it from the external environment after undergoing photo-polymerization, thus effectively assisting in wound hemostasis. Therefore, GGMA-based hydrogels indeed possess rapid hemostatic abilities and excellent adhesive properties, effectively preventing irregular wound bleeding.

3.8. *Therapeutic effects and biocompatibility evaluation of GGMA-based hydrogel on a mouse skin injury model*

We then utilized the GGMA-based hydrogels on a mouse skin injury

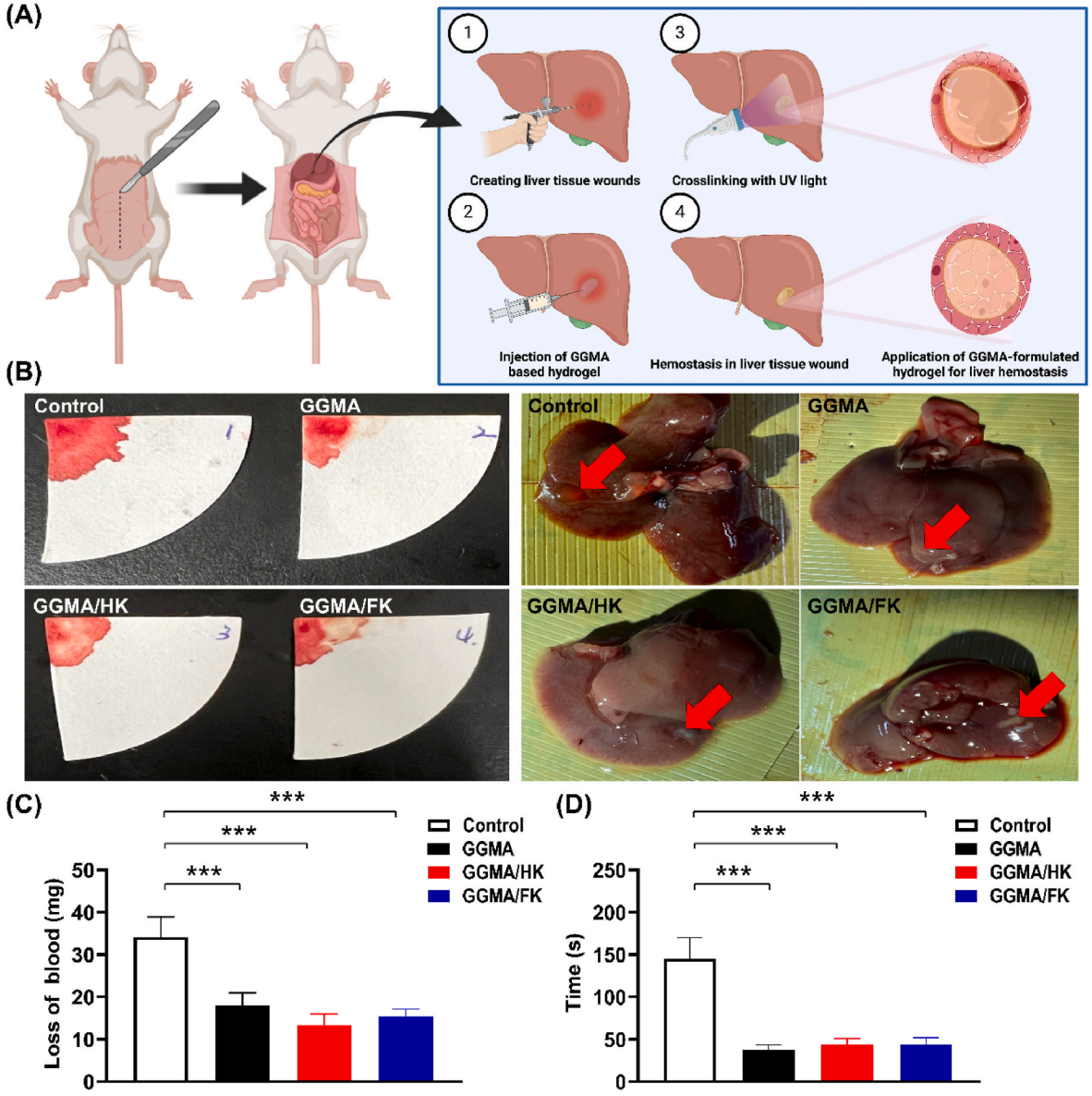

Fig. 5. Utilization of GGMA, GGMA/HK, and GGMA/FK hydrogels for achieving hemostasis in a murine liver puncture model. (A) (1) Construction of a murine liver puncture model. (2) Drops of GGMA, GGMA/HK, and GGMA/FK hydrogels were placed onto the puncture wound site. (3) UV irradiation was employed to induce crosslinking of the hydrogels. (4) Hydrogels transitioned into a solid state, effectively sealing and closing the hemorrhage site. (B) Images of the blood loss of each group (Control, GGMA, GGMA/HK, GGMA/FK) on filter paper. (C, D) Quantification analysis in hemostasis time and residual blood weight on filter paper to assess the impact of these three hydrogels on hemostasis effectiveness for liver injuries. (n = 3) ***$p < 0.001$.

model to evaluate its biocompatibility and therapeutic effects *in vivo* (Fig. 6A). The postoperative photographs showed no evident signs of infection in the skin wound areas or the surrounding skin border treated with three types of hydrogels. While slight redness and swelling were noted at the edges, these symptoms are likely natural responses to the surgical creation of the skin wound model, not directly attributable to the hydrogel (Fig. 6B). Meanwhile, in the groups treated with the hydrogel dressings, a reflective surface at the central area of the wound could be seen, indicating the existence of the hydrogel.

From day 2 to day 8, all groups displayed a reduction in wound area. The central areas of the wounds in the control group appeared dry, with some slight redness, suggesting mild acute inflammation. From day 11 to day 14, the wound areas in all groups had diminished to one-fourth of their original size on day 0, with granulation tissue forming around them. It was noted that the wound area in the GGMA hydrogel group containing keratin was smaller compared to the control group. Although the GGMA group also demonstrated a decreasing trend in wound area, the reduction was less significant than in the other two groups, likely due to differences in wound shape.

On day 17 post-surgery, the condition of all wounds was meticulously examined. It was encouraging to find that all wounds had completely closed. However, while the wounds in the control group had fully healed, a visible scar remained, indicating more effective healing in the GGMA-based hydrogel groups. Further close examination of the central wound areas revealed that the epidermal tissues had fully repaired, restoring a normal skin structure and appearance. Notably, no adverse local tissue reactions, signs of infection, or fluid leakage from the wounds were observed during treatment, affirming the effective

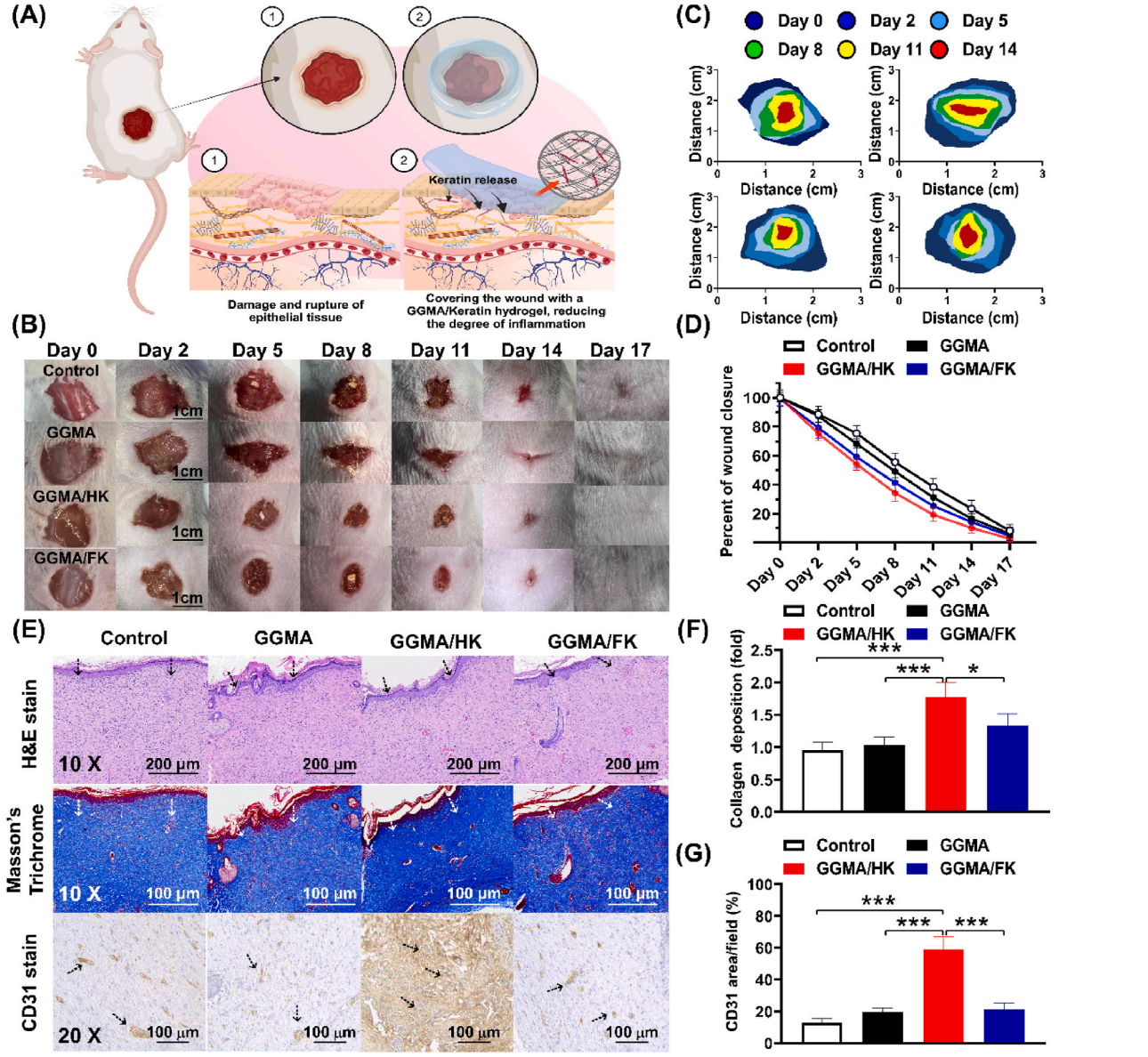

Fig. 6. Treatment of the excisional dorsal full-thickness skin wound using GGMA-based hydrogels. (A) Schematic of the process for fabricating a full-thickness skin wound model and placing a GGMA-based hydrogel on the dorsal wound area. (B) Images of the wound area treated with three types of GGMA-based hydrogels from day 0 to day 17. (C) Simulated analysis of the contraction of mouse skin wounds using three types of hydrogels based on GGMA, and comparing them with the control group. (D) Quantification of the extent of skin wound area contraction from day 0 to day 17. (E) Paraffin skin sections from the treatment with three types of GGMA-based hydrogels and control group on the full-thickness skin wound area of mice were simultaneously subjected to H&E staining, Masson's trichrome staining and immunohistochemical staining (IHC) of CD31 expression for comparisons. (Black and white arrows: wound healing area; black dashed arrow: CD31 expression area). (F, G) Quantitative analysis was conducted to assess the percentage of collagen for Masson's trichrome staining and Immunohistochemical expression of endothelial markers CD31 in each group on day 17. (n = 6) $*p < 0.05$. $***p < 0.001$.

performance of the GGMA-based hydrogels in fostering a conducive environment for natural wound healing.

Photographs taken at each time point were analyzed, and colorized images of the wound area for each time point were produced, showing detailed changes in the wound area, as depicted in Fig. 6C. The group treated with GGMA hydrogel containing keratin showed better wound closure compared to both the GGMA and control groups. We quantified the percentage of wound closure and noted differences between the groups, confirming the effectiveness of GGMA hydrogels containing keratin in wound treatment (Fig. 6D). In the analysis of wound area quantification, the effectiveness of the GGMA/HK group in treating wounds appeared better to that of the GGMA/FK group, suggesting additional benefits of keratin extracted from hair for wound healing.

The typical wound healing process involves stages such as epidermal epithelialization, inflammation, granulation tissue formation, blood vessel generation by endothelial cells, collagen fiber thickening, and dermal tissue remodeling [3,63]. After inspecting the actual skin wound healing condition through H&E staining, we found that on day 17 after surgery, all skin wounds had essentially healed. The newly formed epidermal tissues covered the granulation tissues of the wounds, closely resembling the natural epidermal tissues present in adjacent intact skin. In the control group, despite the complete coverage of the wound area by the epidermal layer, there was no significant thickening observed, and the dermal tissue appeared loosely-structured (Fig. S8). Moreover, the absence of new hair follicles and signs of cellular infiltration were evident, possibly due to the acute inflammatory response in the wound and surrounding granulation tissue from the lack of hydrogel coverage. Conversely, the wounds treated with hydrogels showed significantly thicker epidermal tissues than those in the control group (Fig. 6E). In the GGMA/HK and GGMA/FK groups, we observed a significant thickening of the dermal layer, indicating increased collagen fiber production. Furthermore, the presence of fibroblasts and endothelial cells in the wound area suggests that the repair of the dermis has reached a certain level. On the contrary, the GGMA group displayed loose tissue stacking in the dermal layer. Previous studies indicate that applying keratin peptides to the wound bed can activate keratinocytes in the surrounding wound area, promoting the proliferation and migration of fibroblasts, the production of collagen, and the formation of granulation tissue, thereby advancing to the next stages of wound healing [64]. These studies align with the results of our wound treatment using GGMA/-keratin hydrogels, indicating that GGMA/keratin hydrogels further promoted the wound healing.

During the middle stage of the skin wound healing process, collagen synthesis plays a crucial role by providing a scaffold for wound healing cells and promoting the regeneration of blood vessels, thereby facilitating wound closure [65,66]. Therefore, Masson's trichrome staining was utilized to evaluate collagen fiber remodeling and accumulation in the skin wounds. Through semi-quantitative scoring of Masson's trichrome staining, it was indicated that the expression levels of collagen fiber in the newly formed skin tissue were significantly higher in the GGMA/HK and GGMA/FK groups compared to the control group and the GGMA group. Furthermore, the groups treated with GGMA/HK exhibited superior integrity and collagen expression levels in the newly formed skin tissue, with the collagen fibers appearing thicker and more intact than those in the GGMA/FK group (Fig. 6E). This suggests that GGMA-based hydrogels containing keratin promote the proliferation of collagen fiber in the dermis layer with hair-extracted keratin outperforming feather extracted-keratin (Fig. 6F).

As the wound healing progressed from the middle to the late stages, the presence of vascular endothelial cells and newly formed hair follicles became apparent in the repaired tissue. Therefore, immunohistochemical staining was utilized to evaluate the expression of the vascular endothelial marker CD31, commonly found in tissues rich in blood vessels, for assessing angiogenesis. A concentrated staining phenomenon typically appears between the boundaries of endothelial cells [67]. The quantitative results indicate that in the skin tissues, the expression levels of CD31 in the GGMA, GGMA/HK, and GGMA/FK groups are all higher than those in the control group (Control: 12.66 % ± 2.85 %, GGMA: 19.47 % ± 2.65 %, GGMA/HK: 59.10 % ± 8.01 %, and GGMA/FK: 21.50 % ± 3.7 %) (Fig. 6G). Notably, the CD31 expression in the GGMA/HK group was significantly higher than in the other groups, indicating that hair-derived keratin may contribute to angiogenesis, potentially accelerating tissue repair and enhancing the integrity of newly formed tissue.

Overall, the staining results indicate that GGMA/keratin hydrogels enhance collagen fiber deposition in wound areas, thereby accelerating the skin wound healing process. Additionally, the GGMA/HK hydrogel shows promise in facilitating epithelial cell proliferation, improving tissue integrity, and promoting angiogenesis potential. These findings strongly support the utilization of GGMA/HK hydrogel in wound treatment, underscoring its potential in promoting wound healing. In summary, the application of hydrogel coverage significantly contributes to skin wound repair and fosters neovascularization.

4. Conclusion

Based on the experimental results, we have successfully modified and photo-crosslinked our hydrogel. Incorporation of keratin protein species resulted in hydrogels exhibiting high plasticity, adhesiveness, and biocompatibility. These hydrogels not only possess dense porosity and water absorption traits but can also adjust their stiffness and elasticity, suggesting potential applications in tissue engineering. In the adhesive capability test of hydrogel on tissues, we found that GGMA-based hydrogels exhibit excellent adhesion. They adhere not only to the skin with a certain degree of adhesiveness but also demonstrate outstanding adherence to other organs. Moreover, in a liver puncture injury bleeding model, GGMA-based hydrogels can effectively seal bleeding sites in damaged liver tissue, achieving hemostasis, effectively isolating the wound from external contact. In cell compatibility tests, it was demonstrated that mouse fibroblast cell L929 could adhere and proliferate within a GGMA-based hydrogel containing keratin. Furthermore, confirmation was obtained that the GGMA/HK hydrogel displays excellent cell compatibility, with compatibility levels positively correlating with the presence of keratin. Finally, *in vivo* studies further validated the positive impact of hydrogels on wound healing capabilities. Specifically, GGMA-based hydrogels exhibited remarkable biocompatibility. Additionally, these hydrogels helped maintain a moist environment around the wound, assisting in the growth of granulation tissue for self-debridement of necrotic tissue. Moreover, GGMA/keratin hydrogels delivered keratin factors to damaged areas, aiding in skin repair. Immunohistochemical staining for CD31 expression revealed significant differences between the GGMA/HK-treated skin wounds and other hydrogel groups, indicating that keratin extracted from hair has a certain ability to promote angiogenesis during wound healing. These affirmative outcomes bear implications for wound healing. Collectively, this research paves the way for the development of highly adaptable and controllable biodegradable hydrogels. These accomplishments not only carry a positive influence in the realm of biomedicine but also provide guiding principles and a foundation for tissue engineering and regenerative medicine. Anticipations are that these research findings will introduce greater prospects for future biomaterial design and clinical applications.

CRediT authorship contribution statement

Che-Wei Lin: Writing – original draft, Project administration, Methodology, Investigation. **Tai-Hung Liu:** Writing – review & editing, Validation, Project administration, Formal analysis. **Vincent Chen:** Writing – review & editing, Project administration, Data curation, Conceptualization. **Er-Yuan Chuang:** Supervision, Resources, Funding acquisition. **Yu-Jui Fan:** Supervision, Resources, Funding acquisition. **Jiashing Yu:** Supervision, Investigation, Conceptualization.

Declaration of competing interest

The authors declare that they have no known competing financial interests or personal relationships that could have appeared to influence the work reported in this paper.

Data availability

Data will be made available on request.

Acknowledgement

This project was supported by the National Science and Technology Council, Taiwan (112-2221-E-002 -054 -MY2 and 112-2628-E-002 -017 -MY3), and Ministry of Education, Taiwan. We are appreciative of the Leica TCS SP5 confocal microscope provided by the Technology Commons (TechComm) of the College of Life Science of National Taiwan University. Also, we appreciated the website "Biorender" for supplying graphic elements for experimental scheme production.

Appendix A. Supplementary data

Supplementary data to this article can be found online at https://doi.org/10.1016/j.mtbio.2024.101146.

References

[1] A.B. Johnson, B. Burns, Hemorrhage, 2019.
[2] V. Falanga, R.R. Isseroff, A.M. Soulika, M. Romanelli, D. Margolis, S. Kapp, M. Granick, K. Harding, Chronic wounds, Nat. Rev. Dis. Prim. 8 (1) (2022) 50.
[3] J. Boateng, O. Catanzano, Advanced therapeutic dressings for effective wound healing—a review, J. Pharmaceut. Sci. 104 (11) (2015) 3653–3680.
[4] B.M. Pereira, J.B. Bortoto, G.P. Fraga, Topical hemostatic agents in surgery: review and prospects, Rev. Col. Bras. Cir. 45 (2018).
[5] J. Granville-Chapman, N. Jacobs, M. Midwinter, Pre-hospital haemostatic dressings: a systematic review, Injury 42 (5) (2011) 447–459.
[6] P. Yu, W.J.B. Zhong, trauma, Hemostatic Materials in Wound Care, vol. 9, 2021 tkab019.
[7] A. Duarte, J. Coelho, J. Bordado, M. Cidade, M. Gil, Surgical adhesives: systematic review of the main types and development forecast, Prog. Polym. Sci. 37 (8) (2012) 1031–1050.
[8] X. Yang, W. Liu, N. Li, M. Wang, B. Liang, I. Ullah, A.L. Neve, Y. Feng, H. Chen, C.J. B.S. Shi, Design and development of polysaccharide hemostatic materials and their hemostatic mechanism 5 (12) (2017) 2357–2368.
[9] F.-M. Chen, X. Liu, Advancing biomaterials of human origin for tissue engineering, Prog. Polym. Sci. 53 (2016) 86–168.
[10] J. Koehler, F.P. Brandl, A.M. Goepferich, Hydrogel wound dressings for bioactive treatment of acute and chronic wounds, Eur. Polym. J. 100 (2018) 1–11.
[11] A. Gaspar-Pintiliescu, A.-M. Stanciuc, O. Craciunescu, Natural composite dressings based on collagen, gelatin and plant bioactive compounds for wound healing: a review, Int. J. Biol. Macromol. 138 (2019) 854–865.
[12] N. Gokarneshan, Application of Natural Polymers and Herbal Extracts in Wound Management, Advanced Textiles for Wound Care, 2019, pp. 541–561.
[13] A. Tang, Y. Li, Y. Yao, X. Yang, Z. Cao, H. Nie, G.J.B.S. Yang, Injectable keratin hydrogels as hemostatic and wound dressing materials 9 (11) (2021) 4169–4177.
[14] E. Insuasti-Cruz, V. Suárez-Jaramillo, K.A. Mena Urresta, K.O. Pila-Varela, X. Fiallos-Ayala, S.A. Dahoumane, F.J.A.H.M. Alexis, Natural biomaterials from biodiversity for healthcare applications 11 (1) (2022) 2101389.
[15] R.A.M. Osmani, E. Singh, K. Jadhav, S. Jadhav, R. Banerjee, 23 - biopolymers and biocomposites: nature's tools for wound healing and tissue engineering, in: S. Ahmed (Ed.), Applications of Advanced Green Materials, Woodhead Publishing2021, pp. 573-630.
[16] Y. Liang, Y. Liang, H. Zhang, B. Guo, Antibacterial biomaterials for skin wound dressing, Asian J. Pharm. Sci. 17 (3) (2022) 353–384.
[17] K. Elkhoury, C.S. Russell, L. Sanchez-Gonzalez, A. Mostafavi, T.J. Williams, C. Kahn, N.A. Peppas, E. Arab-Tehrany, A. Tamayol, Soft-nanoparticle functionalization of natural hydrogels for tissue engineering applications, Adv. Healthcare Mater. 8 (18) (2019) 1900506.
[18] R.C. Op't Veld, X.F. Walboomers, J.A. Jansen, F.A. Wagener, Design considerations for hydrogel wound dressings: strategic and molecular advances, Tissue Eng. B Rev. 26 (3) (2020) 230–248.
[19] J. Yang, R. Bai, B. Chen, Z. Suo, Hydrogel adhesion: a supramolecular synergy of chemistry, topology, and mechanics, Adv. Funct. Mater. 30 (2) (2020) 1901693.
[20] Y. Yuan, S. Shen, D.J.B. Fan, A physicochemical double cross-linked multifunctional hydrogel for dynamic burn wound healing: shape adaptability, injectable self-healing property and enhanced adhesion 276 (2021) 120838.
[21] P. Lin, S. Ma, X. Wang, F. Zhou, Molecularly engineered dual-crosslinked hydrogel with ultrahigh mechanical strength, toughness, and good self-recovery, Adv. Mater. 27 (12) (2015) 2054–2059.
[22] L. Tavagnacco, E. Chiessi, L. Severini, S. Franco, E. Buratti, A. Capocefalo, F. Brasili, A. Mosca Conte, M. Missori, R. Angelini, Molecular origin of the two-step mechanism of gellan aggregation, Sci. Adv. 9 (10) (2023) eadg4392.
[23] M. Matsusaki, H. Ikeguchi, C. Kubo, H. Sato, Y. Kuramochi, D. Takagi, Fabrication of perfusable pseudo blood vessels by controlling sol–gel transition of gellan gum templates, ACS Biomater. Sci. Eng. 5 (11) (2019) 5637–5643.
[24] A.H. Bacelar, J. Silva-Correia, J.M. Oliveira, R.L. Reis, Recent progress in gellan gum hydrogels provided by functionalization strategies, J. Mater. Chem. B 4 (37) (2016) 6164–6174.
[25] T. Osmałek, A. Froelich, S. Tasarek, Application of gellan gum in pharmacy and medicine, Int. J. Pharm. 466 (1–2) (2014) 328–340.
[26] T. Muthukumar, J.E. Song, G.J.M. Khang, Biological role of gellan gum in improving scaffold drug delivery, cell adhesion properties for tissue engineering applications 24 (24) (2019) 4514.
[27] S. Dhar, P. Murawala, A. Shiras, V. Pokharkar, B. Prasad, Gellan gum capped silver nanoparticle dispersions and hydrogels: cytotoxicity and in vitro diffusion studies, Nanoscale 4 (2) (2012) 563–567.
[28] H. Warren, M. in het Panhuis, Highly conducting composite hydrogels from gellan gum, PEDOT: PSS and carbon nanofibres, Synth. Met. 206 (2015) 61–65.
[29] F. Wang, Y. Wen, T. Bai, The composite hydrogels of polyvinyl alcohol–gellan gum-Ca2+ with improved network structure and mechanical property, Mater. Sci. Eng. C 69 (2016) 268–275.
[30] J. Silva-Correia, J.M. Oliveira, S.G. Caridade, J.T. Oliveira, R.A. Sousa, J.F. Mano, R.L. Reis, Gellan gum-based hydrogels for intervertebral disc tissue-engineering applications, Journal of Tissue Engineering and Regenerative Medicine 5 (6) (2011) e97–e107.
[31] C.W. Lin, P.T. Wu, E.Y. Chuang, Y.J. Fan, J. Yu, Design and investigation of an eco-friendly wound dressing composed of green bioresources-soy protein, tapioca starch, and gellan gum, Macromol. Biosci. 22 (12) (2022) 2200288.
[32] Z.T. Xie, J. Zeng, D.H. Kang, S. Saito, S. Miyagawa, Y. Sawa, M. Matsusaki, 3D printing of collagen scaffold with enhanced resolution in a citrate-modulated gellan gum microgel bath, Adv. Healthcare Mater. 12 (27) (2023) 2301090.
[33] J.S. Baek, C. Carlomagno, T. Muthukumar, D. Kim, J.H. Park, J.E. Song, C. Migliaresi, A. Motta, R.L. Reis, G.J.M.R. Khang, Evaluation of cartilage regeneration in gellan gum/agar blended hydrogel with improved injectability 27 (2019) 558–564.
[34] Y. Zheng, Y. Liang, D. Zhang, X. Sun, L. Liang, J. Li, Y.-N. Liu, Gelatin-based hydrogels blended with gellan as an injectable wound dressing, ACS Omega 3 (5) (2018) 4766–4775.
[35] A. Das, A. Das, A. Basu, P. Datta, M. Gupta, A. Mukherjee, Newer guar gum ester/chicken feather keratin interact films for tissue engineering, Int. J. Biol. Macromol. 180 (2021) 339–354.
[36] B. Wang, W. Yang, J. McKittrick, M.A. Meyers, Keratin: structure, mechanical properties, occurrence in biological organisms, and efforts at bioinspiration, Prog. Mater. Sci. 76 (2016) 229–318.
[37] S. Pradhan, A. Brooks, V. Yadavalli, Nature-derived materials for the fabrication of functional biodevices, Materials Today Bio 7 (2020) 100065.
[38] E. Ranjit, S. Hamlet, R. George, A. Sharma, R.M. Love, Biofunctional approaches of wool-based keratin for tissue engineering, J. Sci.: Advanced Materials and Devices 7 (1) (2022) 100398.
[39] A. Vasconcelos, A. Cavaco-Paulo, The use of keratin in biomedical applications, Curr. Drug Targets 14 (5) (2013) 612–619.
[40] Y. Wang, W. Zhang, J. Yuan, J. Shen, Differences in cytocompatibility between collagen, gelatin and keratin, Mater. Sci. Eng. C 59 (2016) 30–34.
[41] C. Sun, W. Liu, L. Wang, R. Meng, J. Deng, R. Qing, B. Wang, S. Hao, Photopolymerized keratin-PGLa hydrogels for antibiotic resistance reversal and enhancement of infectious wound healing, Materials Today Bio 23 (2023) 100807.
[42] L.R. Burnett, M.B. Rahmany, J.R. Richter, T.A. Aboushwareb, D. Eberli, C.L. Ward, G. Orlando, R.R. Hantgan, M.E. Van Dyke, Hemostatic properties and the role of cell receptor recognition in human hair keratin protein hydrogels, Biomaterials 34 (11) (2013) 2632–2640.
[43] L.A. Pace, J.F. Plate, S. Mannava, J.C. Barnwell, L.A. Koman, Z. Li, T.L. Smith, M. Van Dyke, A human hair keratin hydrogel scaffold enhances median nerve regeneration in nonhuman primates: an electrophysiological and histological study, Tissue Eng. 20 (3–4) (2014) 507–517.
[44] C.W. Lin, Y.K. Chen, K.C. Tang, K.C. Yang, N.C. Cheng, J. Yu, Keratin scaffolds with human adipose stem cells: physical and biological effects toward wound healing, Journal of tissue engineering and regenerative medicine 13 (6) (2019) 1044–1058.
[45] J. Passipieri, H. Baker, M. Siriwardane, M.D. Ellenburg, M. Vadhavkar, J.M. Saul, S. Tomblyn, L. Burnett, G.J. Christ, Keratin hydrogel enhances in vivo skeletal muscle function in a rat model of volumetric muscle loss, Tissue Eng. 23 (11–12) (2017) 556–571.
[46] W. Li, F. Gao, J. Kan, J. Deng, B. Wang, S. Hao, Synthesis and fabrication of a keratin-conjugated insulin hydrogel for the enhancement of wound healing, Colloids Surf. B Biointerfaces 175 (2019) 436–444.
[47] M. Park, H.K. Shin, B.-S. Kim, M.J. Kim, I.-S. Kim, B.-Y. Park, H.-Y. Kim, Effect of discarded keratin-based biocomposite hydrogels on the wound healing process in vivo, Mater. Sci. Eng. C 55 (2015) 88–94.
[48] W. Ye, M. Qin, R. Qiu, J. Li, Keratin-based wound dressings: from waste to wealth, Int. J. Biol. Macromol. 211 (2022) 183–197.
[49] H. Shin, B.D. Olsen, A. Khademhosseini, The mechanical properties and cytotoxicity of cell-laden double-network hydrogels based on photocrosslinkable

gelatin and gellan gum biomacromolecules, Biomaterials 33 (11) (2012) 3143–3152.
[50] Z. Xu, Z. Li, S. Jiang, K.M. Bratlie, Chemically modified gellan gum hydrogels with tunable properties for use as tissue engineering scaffolds, ACS Omega 3 (6) (2018) 6998–7007.
[51] X.-C. Yin, F.-Y. Li, Y.-F. He, Y. Wang, R.-M. Wang, Study on effective extraction of chicken feather keratins and their films for controlling drug release, Biomater. Sci. 1 (5) (2013) 528–536.
[52] F.D. Martinez-Garcia, T. Fischer, A. Hayn, C.T. Mierke, J.K. Burgess, M.C. Harmsen, A beginner's Guide to the characterization of hydrogel microarchitecture for cellular applications, Gels 8 (9) (2022).
[53] Z. Kaberova, E. Karpushkin, M. Nevoralová, M. Vetrík, M. Šlouf, M. Dušková-Smrčková, Microscopic structure of swollen hydrogels by scanning electron and light microscopies: artifacts and reality, Polymers 12 (3) (2020) 578.
[54] Y. Wei, A.A. Thyparambil, R.A. Latour, Protein helical structure determination using CD spectroscopy for solutions with strong background absorbance from 190 to 230 nm, Biochim. Biophys. Acta Protein Proteonomics 1844 (12) (2014) 2331–2337.
[55] C.R. Robbins, C.R. Robbins, Chemical and Physical Behavior of Human Hair, Springer2012.
[56] Y. Tsuda, Y. Nomura, Properties of alkaline-hydrolyzed waterfowl feather keratin, Anim. Sci. J. 85 (2) (2014) 180–185.
[57] C.R. Chilakamarry, S. Mahmood, S. Saffe, M.A.B. Arifin, A. Gupta, M.Y. Sikkandar, S.S. Begum, B. Narasaiah, Extraction and application of keratin from natural resources: a review, 3 Biotech 11 (5) (2021) 220.
[58] Y. Ma, X. Wang, T. Su, F. Lu, Q. Chang, J. Gao, Recent advances in macroporous hydrogels for cell behavior and tissue engineering, Gels 8 (10) (2022) 606.
[59] Y.S. Zhang, A. Khademhosseini, Advances in engineering hydrogels, Science 356 (6337) (2017).
[60] T.C. Ho, C.C. Chang, H.P. Chan, T.W. Chung, C.W. Shu, K.P. Chuang, T.H. Duh, M. H. Yang, Y.C. Tyan, Hydrogels: properties and applications in biomedicine, Molecules 27 (9) (2022).
[61] S. Uxa, P. Castillo-Binder, R. Kohler, K. Stangner, G.A. Müller, K. Engeland, Ki-67 gene expression, Cell Death Differ. 28 (12) (2021) 3357–3370.
[62] S. Wang, F. Taraballi, L.P. Tan, K.W. Ng, Human keratin hydrogels support fibroblast attachment and proliferation in vitro, Cell Tissue Res. 347 (3) (2012) 795–802.
[63] R.B. Diller, A.J. Tabor, The role of the extracellular matrix (ECM) in wound healing: a review, Biomimetics 7 (3) (2022) 87.
[64] M.P. Than, R.A. Smith, C. Hammond, R. Kelly, C. Marsh, A.D. Maderal, R. S. Kirsner, Keratin-based wound care products for treatment of resistant vascular wounds, The Journal of clinical and aesthetic dermatology 5 (12) (2012) 31.
[65] S.S. Mathew-Steiner, S. Roy, C.K. Sen, Collagen in wound healing, Bioengineering 8 (5) (2021) 63.
[66] S. Chattopadhyay, R.T. Raines, Collagen-based biomaterials for wound healing, Biopolymers 101 (8) (2014) 821–833.
[67] S. Lee, C.M. Valmikinathan, J. Byun, S. Kim, G. Lee, N. Mokarram, S.B. Pai, E. Um, R.V. Bellamkonda, Y.-s. Yoon, Enhanced therapeutic neovascularization by CD31-expressing cells and embryonic stem cell-derived endothelial cells engineered with chitosan hydrogel containing VEGF-releasing microtubes, Biomaterials 63 (2015) 158–167.